

Effective dynamics and fluctuations of a trapped probe moving in a fluid of active hard discs

ASHREYA JAYARAM and THOMAS SPECK

Institute for Theoretical Physics IV, University of Stuttgart, 70569 Stuttgart, Germany

*** Missing PACS ***

Abstract –We study the dynamics of a single trapped probe surrounded by self-propelled active particles in two dimensions. In the limit of large size separation, we perform an adiabatic elimination of the small active particles to obtain an effective Markovian dynamics of the large probe, yielding explicit expressions for the mobility and diffusion coefficient. To calculate these expressions, we perform computer simulations employing active Brownian discs and consider two scenarios: non-interacting bath particles and purely repulsive interactions modeling volume exclusion. We keep the probe-to-bath size ratio fixed and vary the propulsion speed of the bath particles. The positional fluctuations of a trapped probe are accessible in experiments, for which we test the prediction from the adiabatic elimination. Although the approximations cause a discrepancy at equilibrium, the overall agreement between predicted and measured probe fluctuations is very good at larger speeds.

Introduction. – The motion of a solvated colloidal particle is due to a myriad of collisions with the surrounding solvent molecules. Observing only the position of the particle necessarily implies a stochastic process, which for a passive solvent is restricted by statistical physics through the Einstein relation (a special case of the more general fluctuation-dissipation theorem [1]). Due to the scale separation, the collisions become essentially uncorrelated on the time scale of the (much bigger) colloidal particle and typically are modeled as white noise (although deviations can be detected experimentally [2]). Colloidal probes can also be employed to study local properties of complex fluids and heterogeneous biological materials through the probe’s fluctuations [3, 4]. Here one distinguishes between passive and active microrheology, whereby in the later case the probe is driven externally (linearly or oscillatory) [5–7]. The response to a driven probe is governed by the deformation of the microstructure, the statistical arrangement of bath particles around the probe, which has been studied in detail for a bath of hard passive particles [8].

Recently, the concept of *active fluids*, in which constituent particles move autonomously by incessantly transforming residual or stored free energy into directed motion and dissipating heat, has gained traction [9, 10]. The directed motion can be rotational (“spinners”) [11, 12] or linear (self-propulsion) [13], which are distinguished as ac-

tive chiral [14, 15], scalar [16], and polar fluids [17, 18]. The behavior of embedded passive particles in such synthetic active fluids, in addition to bacterial suspensions, has attracted enormous interest [19, 20]. For example, asymmetric probe particles embedded in an active fluid can be used to extract useful work [21–23]. The statistics of symmetric colloidal probes has been measured in experiments [24–26] and effective equations of motion for the probe particle have been derived [27–29]. Moreover, the extent to which the fluctuation-dissipation theorem is violated can be exploited to probe the environment [30–34]. Brady and coworkers have worked out consequences of a driven probe [35, 36]. Special situations such as (anomalous) tracer diffusion in one dimension [37, 38] and at high densities have been explored theoretically [39].

Motivated by recent experiments [40, 41], here we study the motion of a trapped passive probe surrounded by self-propelled active particles [Fig. 1(a)]. In the experiments, the probe is trapped by optical tweezers and the active particles are strongly confined light-driven Janus colloidal particles moving effectively in two dimensions in a binary near-critical solvent [42]. Knowing the trap stiffness, forces onto the probe can be related to the displacement from the trap center.

Solon and Horowitz have studied the relationship between diffusion coefficient and mobility of a probe moving in a bath modeled as active Brownian particles [43]. They

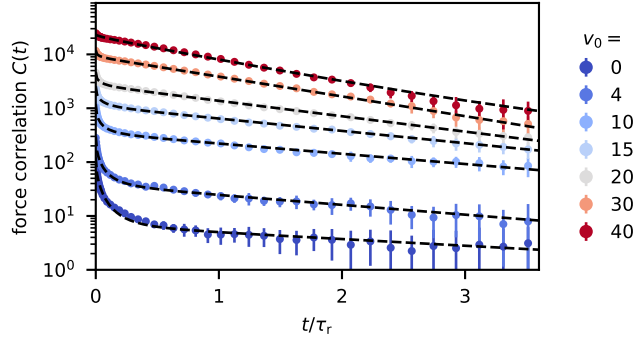


Fig. 1: Probe in active bath. (a) Sketch of the system. A disc-shaped probe is trapped by, e.g., optical tweezers and moving in a bath of active Janus particles. (b) Force autocorrelations $C(t)$ of a fixed probe for several propulsion speeds v_0 of the active bath particles. Lines are fits to Eq. (7) describing a fast relaxation followed by a slower exponential relaxation.

have compared a passive fluid and an active fluid with constant (relatively small) propulsion speed of the active particles and varied the size ratio. Here we fix the size ratio and investigate a large range of propulsion speeds, determining in independent simulations the force correlations and the effective drag on the probe. We then turn to a trapped particle since this is a relevant experimental strategy to probe complex non-equilibrium environments.

Model. — We study a two-dimensional system composed of N active particles and a single probe trapped in a harmonic potential with stiffness k . The overdamped dimensionless equations of motion for the active particles read

$$\dot{\mathbf{r}}_k = \varepsilon^{-1}(v_0 \mathbf{e}_k + \mathbf{F}_k) + \sqrt{2\varepsilon^{-1}} \boldsymbol{\xi}_k. \quad (1)$$

Here, $\varepsilon \equiv \mu_p/\mu_a \ll 1$ is the ratio between the bare mobility μ_p of the probe and the bare mobility μ_a of the active particles. We measure energies in units of $k_B T$, lengths in units of σ (taken as the diameter of the active particles), and time in units of $\sigma^2/(k_B T \mu_p)$. The propulsion speed is v_0 along the unit directions \mathbf{e}_k , which undergo rotational diffusion. With D_r being the (dimensionful) rotational diffusion coefficient, $\tau_r = \varepsilon \tilde{\tau}_r = k_B T \mu_p / (D_r \sigma^2)$ is the dimensionless time over which orientational correlations decay. No-slip boundary conditions (as relevant for self-propelled colloidal particles) imply that rotational and translational diffusion couple with $\tilde{\tau}_r = 1/3$. Finally, the translational Gaussian noise $\boldsymbol{\xi}_k$ has zero mean and unit variance. In practice, we perform simulations of the active particles with mobility ε^{-1} and speed $\varepsilon^{-1}v_0$.

The force $\mathbf{F}_k = -\nabla_k U$ is composed of the repulsive forces with pair potential $u_b(r)$ due to neighboring particles and due to the probe with potential $u_p(r)$. The total potential thus reads $U = \sum_k u_p(|\mathbf{r}_k - \mathbf{r}|) + \sum_{k < l} u_b(|\mathbf{r}_k - \mathbf{r}_l|)$. We will study two scenarios: non-interacting active bath particles with $u_b = 0$ and (almost) hard discs for which we employ the repulsive Weeks-Chandler-Andersen

potential given by ($i = b, p$)

$$u_i(r) = 4\epsilon \left[\left(\frac{\sigma_i}{r} \right)^{12} - \left(\frac{\sigma_i}{r} \right)^6 + \frac{1}{4} \right] \Theta(2^{1/6} \sigma_i - r) \quad (2)$$

to penalize overlaps between any two particles. Here $\Theta(\cdot)$ is the Heaviside step function and we set $\epsilon = 100$ with $\sigma_b = 1$ and $\sigma_p = (1 + \varepsilon^{-1})/2$, and vary the speed v_0 . In both scenarios, bath particles and probe interact through their excluded area and the displacement \mathbf{r} of the probe from the trap center evolves according to

$$\dot{\mathbf{r}} = -k\mathbf{r} + \mathbf{F} + \sqrt{2}\boldsymbol{\xi} \quad (3)$$

with force $\mathbf{F} \equiv \sum_k \mathbf{f}(\mathbf{r}_k - \mathbf{r})$ onto the probe and $\mathbf{f} = -\nabla u_p$. Again, the translational Gaussian noise $\boldsymbol{\xi}$ has zero mean and unit variance.

Fluids of interacting repulsive active Brownian discs are known to undergo motility-induced phase separation (MIPS) at sufficiently high speeds, which results in the co-existence of dilute and dense regions [44]. Here we study a moderate global density $\bar{\rho} = N/A = 0.2$ corresponding to a packing fraction of about 16%. While for speeds $v_0 \gtrsim 100$ the system crosses the binodal into the two-phase region, for these low packing fractions nucleation of the dense phase is strongly suppressed and the fluid remains homogeneous (albeit metastable) [45].

Effective dynamics. — In the appendix, we project out the bath degrees of freedom to derive

$$\partial_t \psi = \mu \nabla \cdot (k\mathbf{r} + \mathcal{T} \nabla) \psi \quad (4)$$

governing the evolution of the probability distribution $\psi(\mathbf{r}, t)$ to find the probe displaced by \mathbf{r} from the trap center. This equation is isomorphic to a passive probe with mobility $\mu \equiv (1 + \zeta)^{-1}$ and effective temperature

$$\mathcal{T} \equiv \frac{1 + D}{1 + \zeta}. \quad (5)$$

While we will see that ζ is an effective drag due to the bath, the coefficient

$$D = \int_0^\infty dt C(t), \quad \langle F_i(t) F_j(0) \rangle_0 = C(t) \delta_{ij} \quad (6)$$

is related to the autocorrelations of the force \mathbf{F} onto a *fixed* probe. Due to symmetry, the correlation matrix reduces to a diagonal matrix with function $C(t)$. The adiabatic elimination predicts the fluctuation-dissipation relation $D_{\text{eq}} = \zeta_{\text{eq}}$ in thermal equilibrium, which implies $\mathcal{T} = 1$ in our units as expected.

Force autocorrelations. — We first turn to the calculation of D [Eq. (6)], for which we consider a fixed probe ($\dot{\mathbf{r}} = 0$) immersed in the active bath. We perform Brownian dynamics simulations of the active particles moving in a square box of edge length L with periodic boundary conditions. Throughout, we set the mobility ratio to $\varepsilon = 0.1$ corresponding to a size ratio of 10.

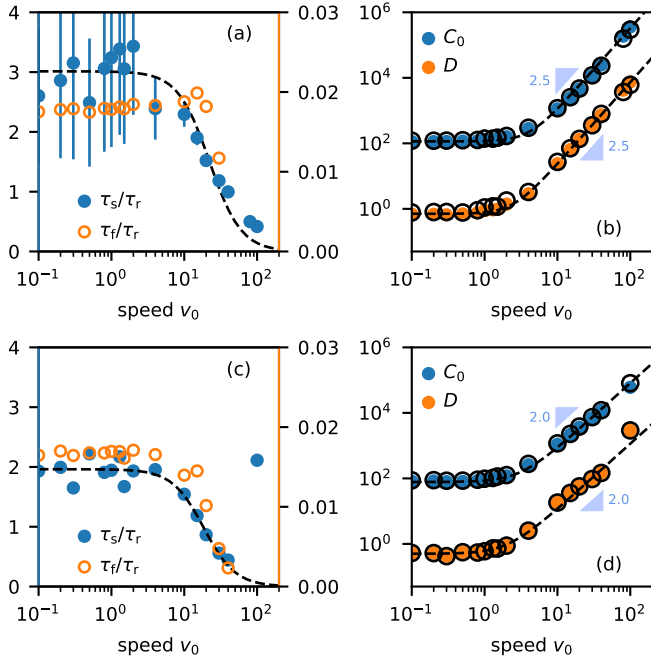


Fig. 2: Analysis of force correlations. (a) Fitted relaxation times τ_s (left axis) and τ_f (right axis) divided by the rotational relaxation time τ_r as a function of speed v_0 . While τ_s is of order τ_r , the fast relaxation $\tau_f \ll \tau_s$ is two orders of magnitude faster. The dashed line is a fit to Eq. (8). (b) The increase of the static force correlations C_0 and the integral D follow a power law as a function of propulsion speed with exponent $\nu = 2.5$ (dashed lines). The open circles indicate the values calculated from the fits [Eq. (7)]. (c,d) Same analysis but now for a bath of non-interacting active discs.

Figure 1(b) reveals that the numerical force correlations $C(t)$ exhibit a two-step decay, which is well fitted by the function

$$C(t) = \frac{D_s}{\tau_s} e^{-t/\tau_s} + \frac{D_f}{2\tau_f} e^{-\sqrt{t/\tau_f}}. \quad (7)$$

This functional form can be interpreted as a slow exponential relaxation on timescale τ_s separated from a spectrum of fast exponential timescales giving rise to a stretched exponential with exponent $\approx 1/2$. While the slow timescale should be related to diffusion, the origin of the fast timescale is the interactions between probe and bath particles since the non-interacting bath particles show the same two-step decay. Note that our data is not compatible with a power-law decay as suggested in [43]. For large speeds, the fast relaxation effectively vanishes. For even higher speeds $v_0 \gtrsim 100$, the statistics become insufficient even for intermediate times with a narrow window of fast decay.

In Fig. 2(a), we plot the fitted relaxation times. While τ_s is of order τ_r and thus determined by the decay of the orientational correlations of the active particles around the probe, the fast relaxation times τ_f are two orders of magnitude smaller. Both time scales have vanishing slope for small speeds (notwithstanding the large uncertainty of

τ_f) and decay for large propulsion speed, which we will see corresponds to an “active thinning” of the bath. Assuming that the slow decorrelation of forces is determined by an effective diffusion of active particles leads to

$$\tau_s(v_0) = \frac{\ell^2}{D_{\text{eff}}(v_0)} = \frac{\tau_{\text{eq}}}{1 + (v_0/v_\tau)^2} \quad (8)$$

with length $\ell \equiv \sqrt{D_{\text{eff}}(0)\tau_{\text{eq}}}$ and assuming that the diffusion coefficient increases quadratically. This functional form yields a reasonable fit to the data for interacting active discs [Fig. 2(a)] with $\tau_{\text{eq}} \simeq 3.0$ and crossover speed $v_\tau \simeq 22.2$. A bath of non-interacting active discs ($u_b = 0$) behaves qualitatively similar as shown in Fig. 2(c) with slight different fit parameters $\tau_{\text{eq}} \simeq 2.0$ and $v_\tau \simeq 18.5$.

In Fig. 2(b), we show the static force correlations C_0 together with the time integral of the force correlations $D = D_s + D_f$ as a function of propulsion speed v_0 . Interestingly, both quantities seem to increase as a power law (i.e., $D - D_{\text{eq}} \propto v_0^\nu$) with an exponent close to $\nu \simeq 5/2$. We also calculate the corresponding values from the fitted correlation functions [Eq. (7)], which agree well with the directly determined values. For non-interacting active discs [Fig. 2(d)], the most notable difference is the change of exponent for the increase of the static and integrated force correlation C_0 and D , respectively, which are now better described by an exponent $\nu \simeq 2$.

Driven probe. – In order to calculate the mobility, we now consider a probe moving according to

$$\mathbf{u} = \dot{\mathbf{r}} = f_p \mathbf{e}_x + \mathbf{F} \quad (9)$$

driven by a constant force f_p along the direction \mathbf{e}_x . Introducing the mobility μ through $\langle \mathbf{u} \rangle = \mu f_p \mathbf{e}_x$ and writing $\langle \mathbf{F} \rangle = -\zeta \langle \mathbf{u} \rangle$, we confirm the relation $\mu = (1 + \zeta)^{-1}$ between mobility μ and the drag coefficient ζ .

To accommodate the anticipated deformation of the average arrangement of bath particles around the probe, simulations are performed in an elongated box with dimensions $L_x = 5L_y$. For small v_0 , as shown in Fig. 3(a,b), the dragged probe witnesses an accumulation of active particles ahead of it and leaves behind a pronounced wake similar to a bath of passive hard discs [8]. The span of the wake increases as f_p increases. For larger v_0 , the distribution of particles around the probe remains homogeneous for small f_p and becomes inhomogeneous for larger driving force f_p , cf. Fig. 3(c,d).

We perform a series of simulations for each propulsion speed v_0 increasing the driving force f_p . We determine

$$\mu = \lim_{f_p \rightarrow 0} \frac{\langle u_x \rangle}{f_p}, \quad \zeta = - \lim_{f_p \rightarrow 0} \frac{\langle F_x \rangle}{\langle u_x \rangle} \quad (10)$$

from independent measurements of speed and force. These are plotted in Fig. 3(e) for interacting and in Fig. 3(f) for non-interacting bath particles. The relation $\mu = (1 + \zeta)^{-1}$ is obeyed as expected. For $v_0 \rightarrow 0$, we expect $D_{\text{eq}} = \zeta_{\text{eq}}$, which, however, is not obeyed. This failure indicates that

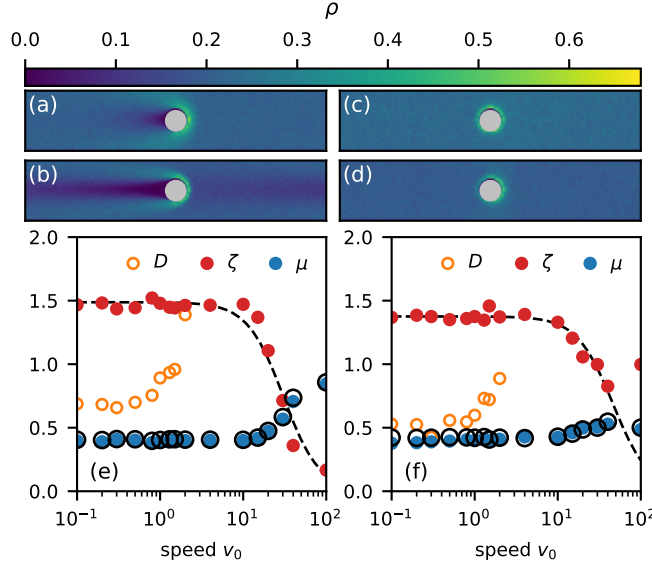


Fig. 3: Driven probe. Density distributions of active particles around the probe for (a) $v_0 = 10$, $f_p = 40$, (b) $v_0 = 10$, $f_p = 200$, (c) $v_0 = 200$, $f_p = 40$, and (d) $v_0 = 200$, $f_p = 200$. (e) Drag coefficient ζ and mobility μ as a function of speed for interacting bath particles. The dashed line is a fit to Eq. (11). The open circles indicate $(1 + \zeta)^{-1}$, which agree with the mobility as predicted. Also shown are the integrated force correlations D . (f) Same as panel (e) but for non-interacting bath particles.

the approximations underlying Eq. (4) are not (yet) fulfilled for the mobility ratio $\varepsilon = 0.1$. Interestingly, this holds for both interacting and non-interacting bath particles.

The drag coefficient ζ remains approximately constant for small v_0 and drops beyond $v_0 \gtrsim 10$. Active baths at high propulsion speed thus exert a reduced drag (“active thinning”) in agreement with previous results obtained by Burkholder and Brady [35]. We observe that the data is well fitted by

$$\zeta(v_0) = \frac{\zeta_{\text{eq}}}{1 + (v_0/v_\zeta)^2} \quad (11)$$

in analogy with the reduction of the slow timescale [Eq. (8)]. Again, both interacting and non-interacting bath particles behave similarly.

Steady state fluctuations. – Having calculated the two coefficients D and ζ , we now turn to the steady-state fluctuations $\chi \equiv \langle \mathbf{r}^2 \rangle$ of the moving probe confined by a quadratic potential. In equilibrium, the partition function

$$Z(k) = \int d^2\mathbf{r} d^2\mathbf{r}_1 \dots e^{-(U + \frac{1}{2}k\mathbf{r}^2)} = \frac{2\pi}{k} Z_b \quad (12)$$

factorizes after shifting positions $\mathbf{r}_k \rightarrow \mathbf{r}_k + \mathbf{r}$. The second moment $\chi_{\text{eq}} = \langle \mathbf{r}^2 \rangle_{\text{eq}} = -2\partial_k \ln Z(k) = 2/k$ is thus independent of the bath–probe interactions. Multiplying Eq. (4) by \mathbf{r}^2 and performing integration by parts twice, we obtain $\chi = (2/k)\mathcal{T}$, which reduces to the equilibrium

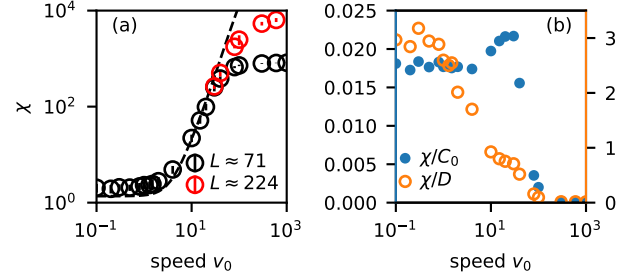


Fig. 4: Probe fluctuations in a trap with stiffness $k = 1$. (a) Averaged squared distance $\chi = \langle \mathbf{r}^2 \rangle$ to the trap center as a function of propulsion speed v_0 . Shown are two system sizes. The dashed line is the prediction $2\mathcal{T}$ from the effective dynamics together with Eq. (5). (b) Reduced fluctuations with respect to C_0 and D .

result for $v_0 = 0$. Note that from Eq. (3) we can derive the exact relation $k\langle \mathbf{r}^2 \rangle = 2 + \langle \mathbf{r} \cdot \mathbf{F} \rangle$, which implies another expression $\mathcal{T} = 1 + \langle \mathbf{r} \cdot \mathbf{F} \rangle / 2$ for the effective temperature.

In Fig. 4(a), we plot χ as a function of propulsion speed for $k = 1$. Simulations are again performed in a square box but now the probe moves according to Eq. (3). The positional fluctuations start at $\chi_{\text{eq}} = 2$ and then rise quickly before saturating at large speeds. This saturation is a finite-size effect as the fluctuations $\chi \sim L^2$ reach the box size, which is confirmed by simulating a larger system size shifting the saturation to larger values of χ [red symbols in Fig. 4(a)]. We also plot the prediction $2\mathcal{T}$ from the effective dynamics using the functional forms for D and ζ in Eq. (5) together with the fitted parameters. This prediction agrees very well with the simulation results except for small speeds, where it underestimates the correct value of 2 due to the violation of the fluctuation-dissipation relation $D_{\text{eq}} = \zeta_{\text{eq}}$.

In Fig. 4(b), we show how the fluctuations χ behave as a function of the static and integrated force correlation. We find a constant factor $\chi/C_0 \simeq 0.018$ up to speeds $v_0 \lesssim 10$, which shows that the static force correlations are well correlated with the positional fluctuations. This correlation is much less pronounced with the integrated force correlations D .

Conclusions. – Probing complex environments out of equilibrium, such as living matter, requires reliable models to interpret the data. Observing an optically trapped probe is a feasible experimental strategy, with the probe fluctuations encoding the activity of the environment. Through an adiabatic elimination of bath particles, we have derived the effective memoryless Markovian dynamics [Eq. (4)] of a probe particle moving in an external potential (here a quadratic potential) in a bath of active particles. The small expansion parameter is the mobility ratio and the result should hold for any propulsion speed of the active bath particles. To assess the validity of the effective dynamics, we have performed Brownian

dynamics simulations of hard discs modeled through the WCA potential Eq. (2). Interestingly, we find only rather small differences between non-interacting and interacting bath particles. Our system is characterized by a linear response regime up to propulsion speeds $v_0 \simeq 10$, beyond which it undergoes “active thinning” characterized by a reduced drag coefficient and a power-law increase of force correlations and positional fluctuations. Curiously, the exponent for interacting bath particles seems to be closer to $\nu = 5/2$ while for non-interacting it is $\nu = 2$ more in line with the expected increase of the effective diffusion D_{eff} of the active bath particles. It would be interesting to see if discontinuous thinning is possible as has been observed for strong probe-bath attractions [46].

The effective dynamics is governed by the force correlations, which display a two-step decay to a slow exponential decay [Fig. 1(b)]. In equilibrium, the integrated force correlations should equal the drag coefficient, which is not obeyed in the data for this system [Fig. 3(e,f)], presumably due to replacing the exact expression [Eq. (27)] by an integral over the force correlations [Eq. (28)]. Another possibility is that non-Markovian effects are not negligible, leading to a generalized Langevin equation for which we would have to determine the memory kernel [47–50].

We acknowledge funding by the Deutsche Forschungsgemeinschaft (DFG) within collaborative research center TRR 146 (Grant No. 404840447). Computations have been performed on the supercomputer MOGON II (ZDV Mainz).

Appendix. – For completeness, we now derive the effective evolution equation (4) for the probability $\psi(\mathbf{r}, t)$ of the probe. We perform an adiabatic elimination [51, 52] similar to Ref. [43] but for overdamped probe dynamics and fully accounting for the small expansion parameter ε .

Projection formalism. It will be helpful to explicitly introduce the probe velocity \mathbf{u} as an auxiliary variable so that the probe equations of motion read $\dot{\mathbf{r}} = \mathbf{u}$ and

$$\gamma^{-1} \dot{\mathbf{u}} + \mathbf{u} = -k\mathbf{r} + \mathbf{F} + \sqrt{2}\boldsymbol{\xi} \quad (13)$$

with relaxation time γ^{-1} . We recover the overdamped equation (3) in the limit $\gamma^{-1} \rightarrow 0$. We measure the positions $\mathbf{r}_k = \mathbf{r} + \mathbf{r}'_k$ of bath particles with respect to the probe. The joint probability $\Psi(\{\mathbf{r}'_k, \varphi_k\}, \mathbf{r}, \mathbf{u}; t)$ evolves according to the Smoluchowski equation

$$\partial_t \Psi = \mathcal{L}_p \Psi + \varepsilon^{-1} \mathcal{L}_0 \Psi \quad (14)$$

with differential operators

$$\mathcal{L}_p = -\mathbf{u} \cdot \nabla + \mathcal{L}_u + \gamma(k\mathbf{r} - \mathbf{F}) \cdot \frac{\partial}{\partial \mathbf{u}} + \mathbf{u} \cdot \sum_k \nabla'_k, \quad (15)$$

$$\mathcal{L}_0 = \sum_k \left[-\nabla'_k \cdot (v_0 \mathbf{e}_k + \mathbf{F}_k - \nabla'_k) + \frac{1}{\tilde{\tau}_r} \frac{\partial^2}{\partial \varphi_k^2} \right], \quad (16)$$

and $\mathcal{L}_u = \partial_{\mathbf{u}} \cdot (\gamma \mathbf{u} + \gamma^2 \partial_{\mathbf{u}})$. The advantage of introducing the speed \mathbf{u} is that \mathbf{F}_k , and thus \mathcal{L}_0 , are independent of the explicit probe position \mathbf{r} which simplifies some of the following calculations at the expense of having to eliminate the probe speed afterwards.

Exploiting that ε is small, we aim to eliminate the bath particles and derive an effective evolution equation for the probe. The bath particles assume a stationary distribution $\phi_0(\{\mathbf{r}'_k, \varphi_k\})$ defined through $\mathcal{L}_0 \phi_0 = 0$. Note that \mathcal{L}_0 only acts on relative positions and orientations of the bath particles. Our main tool will be the projection operator

$$\mathcal{P} \circ = \phi_0 \prod_k \int d^2 \mathbf{r}'_k \int_0^{2\pi} d\varphi_k \circ \quad (17)$$

onto the stationary distribution ϕ_0 so that $\mathcal{P} \phi_0 = \phi_0$. Clearly, $\mathcal{L}_0 \mathcal{P} = \mathcal{P} \mathcal{L}_0 = 0$ and we can split

$$\partial_t \Psi_0 = \mathcal{P} \mathcal{L}_p (\Psi_0 + \Psi_1) \quad (18)$$

$$\partial_t \Psi_1 = (1 - \mathcal{P}) \mathcal{L}_p \Psi_0 + [(1 - \mathcal{P}) \mathcal{L}_p + \varepsilon^{-1} \mathcal{L}_0] \Psi_1 \quad (19)$$

with $\Psi_0 = \mathcal{P} \Psi$ and the remainder

$$\Psi_1 = \Psi - \Psi_0 = -\varepsilon \mathcal{L}_0^{-1} (1 - \mathcal{P}) \mathcal{L}_p \Psi_0 + \mathcal{O}(\varepsilon^2) \quad (20)$$

expanded to lowest order of ε . Plugging this expression back into Eq. (18) leads to an evolution equation for Ψ_0 alone.

Eliminating the bath particles. We start by writing

$$\Psi_0 = \mathcal{P} \Psi = \phi_0(\{\mathbf{r}'_k, \varphi_k\}) \psi^u(\mathbf{r}, \mathbf{u}, t), \quad (21)$$

where ψ^u is the marginal probability of probe position and speed that we are interested in. We now inspect all terms to find an evolution equation for ψ^u alone. Turning to $\mathcal{P} \mathcal{L}_p \Psi_0$, the first two terms factorize and $\mathcal{P} \nabla'_k = 0$, leaving

$$\phi_0 \frac{\partial}{\partial \mathbf{u}} \cdot \gamma(k\mathbf{r} - \langle \mathbf{F} \rangle_0) \psi^u \quad (22)$$

with the average force $\langle \mathbf{F} \rangle_0$ onto the probe. Since the bath particles see a stationary probe they assume a symmetric distribution and this force vanishes, $\langle \mathbf{F} \rangle_0 = 0$. We thus find

$$\mathcal{P} \mathcal{L}_p \Psi_0 = \phi_0 \left[-\mathbf{u} \cdot \nabla + \mathcal{L}_u + \gamma k \mathbf{r} \cdot \frac{\partial}{\partial \mathbf{u}} \right] \psi^u \quad (23)$$

and

$$\tilde{\Psi} = (1 - \mathcal{P}) \mathcal{L}_p \Psi_0 = -\phi_0 \gamma \mathbf{F} \cdot \frac{\partial \psi^u}{\partial \mathbf{u}} + \phi_0 \mathbf{G} \cdot \mathbf{u} \psi^u \quad (24)$$

with $\mathbf{G}(\{\mathbf{r}'_k, \varphi_k\}) \equiv \sum_k \nabla'_k \ln \phi_0$.

The next step is to consider

$$\mathcal{P} \mathcal{L}_p \Psi_1 = -\varepsilon \mathcal{P} \mathcal{L}_p \mathcal{L}_0^{-1} \tilde{\Psi} \quad (25)$$

inserting Eq. (20). All terms of \mathcal{L}_p [Eq. (15)] that do not involve \mathbf{r}' commute with the projector and drop out

since $\mathcal{P}\Psi_1 = 0$ has to vanish, as does the last term. The remaining terms are

$$\mathcal{P}\mathcal{L}_p\Psi_1 = \varepsilon\phi_0 \sum_{ij} \left[\gamma\zeta_{ij} \frac{\partial}{\partial u_i} u_j \psi^u + \gamma^2 D_{ij} \frac{\partial^2 \psi^u}{\partial u_i \partial u_j} \right] \quad (26)$$

with tensors

$$D_{ij} \equiv -\langle F_i \mathcal{L}_0^{-1} F_j \rangle_0, \quad \zeta_{ij} \equiv \langle F_i \mathcal{L}_0^{-1} G_j \rangle_0 \quad (27)$$

contributing to the drift and diffusion terms, respectively. Since our original setup is rotationally symmetric, we expect that both reduce to diagonal tensors $D_{ij} = D\delta_{ij}$ and $\zeta_{ij} = \zeta\delta_{ij}$.

Practically, the expressions Eq. (27) involving the inverse evolution operator of the bath are not very useful. To convert these into integrals of correlation functions, we insert unity, $1 = \int_0^\infty ds \delta(s)$, and use that $e^{\mathcal{L}_0 s} \rightarrow -\mathcal{L}_0^{-1} \delta(s)$ in the limit of perfect scale separation when the correlation function approaches a δ -distribution. With this approximation, we transform

$$D_{ij} = -\langle F_i \mathcal{L}_0^{-1} F_j \rangle_0 \approx \int_0^\infty ds \langle F_i e^{\mathcal{L}_0 s} F_j \rangle_0 \quad (28)$$

into the integral of the force correlations of a fixed probe that can be measured in simulations. To make contact with the simulations, we define $\varepsilon D \rightarrow D$ and $\varepsilon \zeta \rightarrow \zeta$ involving $(\varepsilon^{-1} \mathcal{L}_0)^{-1}$ so that the bath corresponds to active discs with speed $\varepsilon^{-1} v_0$ and (dimensionless) mobility ε^{-1} .

For passive systems, we have $\phi_0 \propto e^{-U(\{\mathbf{r}_k\})}$ up to a normalization constant. Calculating \mathbf{G} , the sum of the interparticle forces between bath particles vanishes (Newton's 3rd law) and

$$\mathbf{G}_{\text{eq}} = \sum_{k=1}^N \mathbf{F}_k = -\mathbf{F} \quad (29)$$

is given by the force on the probe. For passive systems we thus have $\zeta_{\text{eq}} = D_{\text{eq}}$ in agreement with the fluctuation-dissipation theorem.

Putting everything together, we find the evolution equation

$$\partial_t \psi^u = (\mathcal{L}'_u + \mathcal{L}'_p) \psi^u \quad (30)$$

for the marginal distribution $\psi^u(\mathbf{r}, \mathbf{u}, t)$ with (intermediate) operators

$$\mathcal{L}'_p = -\mathbf{u} \cdot \nabla + \gamma k \mathbf{r} \cdot \frac{\partial}{\partial \mathbf{u}}, \quad (31)$$

$$\mathcal{L}'_u = \frac{\partial}{\partial \mathbf{u}} \cdot \left[\gamma(1 + \zeta) \mathbf{u} + \gamma^2(1 + D) \frac{\partial}{\partial \mathbf{u}} \right]. \quad (32)$$

Eliminating probe speed. The final step is to eliminate the speed \mathbf{u} in the limit $\gamma^{-1} \rightarrow 0$. This step is performed in analogy to the elimination of bath particles through factorizing $\psi^u(\mathbf{r}, \mathbf{u}, t) = f_0(\mathbf{u})\psi(\mathbf{r}, t)$ with $\mathcal{L}'_u f_0 = 0$. It is straightforward to show that the solution is

$$f_0(\mathbf{u}) = \frac{2\pi}{\alpha} e^{-\alpha \mathbf{u}^2/2}, \quad \frac{\partial f_0}{\partial \mathbf{u}} = -\alpha \mathbf{u} f_0 \quad (33)$$

with coefficient

$$\alpha \equiv \gamma^{-1} \frac{1 + \zeta}{1 + D}. \quad (34)$$

The orthogonal component reads [cf. Eq. (20)]

$$\psi_1 \approx -\mathcal{L}'_u^{-1} (1 - \mathcal{P}_u) \mathcal{L}'_p f_0 \psi \quad (35)$$

with projection operator \mathcal{P}_u onto f_0 . Let us look at $\mathcal{L}'_p f_0 = -f_0 \mathbf{u} \cdot (\nabla + \gamma \alpha k \mathbf{r})$ and thus $\mathcal{P}_u \mathcal{L}'_p f_0 = 0$. Next, $\mathcal{L}'_u \mathbf{u} f_0 = -\gamma(1 + \zeta) \mathbf{u} f_0$ implies

$$\mathcal{L}'_u^{-1} \mathbf{u} f_0 = -\gamma^{-1} (1 + \zeta)^{-1} \mathbf{u} f_0 \quad (36)$$

leading to

$$\begin{aligned} \psi_1 &= (\mathcal{L}'_u^{-1} \mathbf{u} f_0) \cdot (\nabla + \gamma \alpha k \mathbf{r}) \psi \\ &= -\gamma^{-1} (1 + \zeta)^{-1} \mathbf{u} f_0 \cdot (\nabla + \gamma \alpha k \mathbf{r}) \psi. \end{aligned} \quad (37)$$

Whence

$$\begin{aligned} \mathcal{P}_u \mathcal{L}'_p \psi_1 &= -\gamma^{-1} (1 + \zeta)^{-1} f_0 \times \\ &\int d^2 \mathbf{u} f_0 (-\mathbf{u} \mathbf{u} \cdot \nabla + \gamma k \mathbf{r} - \gamma \alpha k \mathbf{r} \cdot \mathbf{u} \mathbf{u}) \cdot (\nabla + \gamma \alpha k \mathbf{r}) \psi \\ &= f_0 (1 + \zeta)^{-1} \nabla \cdot [(\gamma \alpha)^{-1} \nabla + k \mathbf{r}] \psi \end{aligned} \quad (38)$$

employing the Gaussian integral $\int d^2 \mathbf{u} u_i u_j f_0 = \alpha^{-1} \delta_{ij}$. We can now read off the final evolution equation (4), which is independent of γ .

REFERENCES

- [1] CHANDLER D., *Introduction to Modern Statistical Mechanics* (Oxford University Press, New York) 1987.
- [2] FRANOSCH T., GRIMM M., BELUSHKIN M., MOR F. M., FOFFI G., FORRÓ L. and JENEY S., *Nature*, **478** (2011) 85.
- [3] CICUTA P. and DONALD A. M., *Soft Matter*, **3** (2007) 1449.
- [4] WILHELM C., *Phys. Rev. Lett.*, **101** (2008) 028101.
- [5] MIZUNO D., TARDIN C., SCHMIDT C. F. and MACKINTOSH F. C., *Science*, **315** (2007) 370.
- [6] MIZUNO D., HEAD D. A., MACKINTOSH F. C. and SCHMIDT C. F., *Macromolecules*, **41** (2008) 7194.
- [7] WILSON L. G., HARRISON A. W., SCHOFIELD A. B., ARLT J. and POON W. C. K., *J. Phys. Chem. B*, **113** (2009) 3806.
- [8] SQUIRES T. M. and BRADY J. F., *Phys. Fluids*, **17** (2005) 073101.
- [9] SAINTILLAN D., *Annu. Rev. Fluid Mech.*, **50** (2018) 563.
- [10] RAMASWAMY S., *Nat. Rev. Phys.*, **1** (2019) 640.
- [11] KOKOT G., DAS S., WINKLER R. G., GOMPPER G., ARANSON I. S. and SNEZHKO A., *Proc. Natl. Acad. Sci. U.S.A.*, **114** (2017) 12870.
- [12] NGUYEN N. H. P., KLOTSAS D., ENGEL M. and GLOTZER S. C., *Phys. Rev. Lett.*, **112** (2014) .
- [13] ROMANCZUK P., BÄR M., EBELING W., LINDNER B. and SCHIMANSKY-GEIER L., *Eur. Phys. J. Spec. Top.*, **202** (2012) 1.

- [14] BANERJEE D., SOUSLOV A., ABANOV A. G. and VITELLI V., *Nat. Commun.*, **8** (2017) 1573.
- [15] SONI V., BILILIGN E. S., MAGKIRIADOU S., SACANNA S., BARTOLO D., SHELLEY M. J. and IRVINE W. T. M., *Nat. Phys.*, **15** (2019) 1188.
- [16] BUTTINONI I., BIALKÉ J., KÜMMEL F., LÖWEN H., BECHINGER C. and SPECK T., *Phys. Rev. Lett.*, **110** (2013) 238301.
- [17] BRICARD A., CAUSSIN J.-B., DESREUMAUX N., DAUCHOT O. and BARTOLO D., *Nature*, **503** (2013) 95.
- [18] CHARDAC A., HOFFMANN L. A., POUPART Y., GIOMI L. and BARTOLO D., *Phys. Rev. X*, **11** (2021) 031069.
- [19] LEPTOS K. C., GUASTO J. S., GOLLUB J. P., PESCI A. I. and GOLDSTEIN R. E., *Phys. Rev. Lett.*, **103** (2009) 198103.
- [20] MIÑO G., DUNSTAN J., ROUSSELET A., CLÉMENT E. and SOTO R., *J. Fluid Mech.*, **729** (2013) 423.
- [21] SOKOLOV A., APODACA M. M., GRZYBOWSKI B. A. and ARANSON I. S., *Proc. Natl. Acad. Sci. U.S.A.*, **107** (2010) 969.
- [22] DI LEONARDO R., ANGELANI L., DELL'ARCIPRETE D., RUOCCO G., IECCA V., SCHIPPA S., CONTE M. P., MECARINI F., DE ANGELIS F. and DI FABRIZIO E., *Proc. Natl. Acad. Sci. U.S.A.*, **107** (2010) 9541.
- [23] SPECK T. and JAYARAM A., *Phys. Rev. Lett.*, **126** (2021) 138002.
- [24] WU X.-L. and LIBCHABER A., *Phys. Rev. Lett.*, **84** (2000) 3017.
- [25] ORTLIEB L., RAFAÏ S., PEYLA P., WAGNER C. and JOHN T., *Phys. Rev. Lett.*, **122** (2019) 148101.
- [26] KANAZAWA K., SANO T. G., CAIROLI A. and BAULE A., *Nature*, **579** (2020) 364.
- [27] KNEŽEVIĆ M. and STARK H., *New J. Phys.*, **22** (2020) 113025.
- [28] FENG M. and HOU Z., *Effective Dynamics of Tracer in Active Bath: A Mean-field Theory Study* (Oct. 2021).
- [29] TRIPATHI A. K. and TLUSTY T., *Gauging nanoswimmer dynamics via the motion of large bodies* (Oct. 2022).
- [30] BERTHIER L. and KURCHAN J., *Nat. Phys.*, **9** (2013) 310.
- [31] BEN-ISAAC E., FODOR É., VISCO P., VAN WIJLAND F. and GOV N. S., *Phys. Rev. E*, **92** (2015) 012716.
- [32] MAGGI C., PAOLUZZI M., ANGELANI L. and DI LEONARDO R., *Sci Rep*, **7** (2017) 17588.
- [33] YE S., LIU P., YE F., CHEN K. and YANG M., *Soft Matter*, **16** (2020) 4655.
- [34] SHEA J., JUNG G. and SCHMID F., *Soft Matter*, **18** (2022) 6965.
- [35] BURKHOLDER E. W. and BRADY J. F., *Soft Matter*, **16** (2020) 1034.
- [36] PENG Z. and BRADY J. F., *J. Chem. Phys.*, **157** (2022) 104119.
- [37] BANERJEE T., JACK R. L. and CATES M. E., *J. Stat. Mech.*, **2022** (2022) 013209.
- [38] GRANKE O., KAFRI Y. and TAILLEUR J., *Phys. Rev. Lett.*, **129** (2022) 038001.
- [39] REICHERT J. and VOIGTMANN T., *Soft Matter*, **17** (2021) 10492.
- [40] LIU P., YE S., YE F., CHEN K. and YANG M., *Phys. Rev. Lett.*, **124** (2020) 158001.
- [41] PAUL S., JAYARAM A., NARINDER N., SPECK T. and BECHINGER C., *Phys. Rev. Lett.*, **129** (2022) 058001.
- [42] GOMEZ-SOLANO J. R., SAMIN S., LOZANO C., RUEDAS-BATUECAS P., VAN ROIJ R. and BECHINGER C., *Sci. Rep.*, **7** (2017) 14891.
- [43] SOLON A. and HOROWITZ J. M., *J. Phys. A: Math. Theor.*, **55** (2022) 184002.
- [44] CATES M. E. and TAILLEUR J., *Annu. Rev. Condens. Matter Phys.*, **6** (2015) 219.
- [45] RICHARD D., LÖWEN H. and SPECK T., *Soft Matter*, **12** (2016) 5257.
- [46] WULFERT R., SEIFERT U. and SPECK T., *Phys. Rev. E*, **94** (2016) 062610.
- [47] HIJÓN C., ESPAÑOL P., VANDEN-EIJNDEN E. and DELGADO-BUSCALIONI R., *Faraday Discuss.*, **144** (2010) 301.
- [48] JUNG G., HANKE M. and SCHMID F., *J. Chem. Theory Comput.*, **13** (2017) 2481.
- [49] MEYER H., PELAGEJCEV P. and SCHILLING T., *EPL*, **128** (2020) 40001.
- [50] AYAZ C., SCALFI L., DALTON B. A. and NETZ R. R., *Phys. Rev. E*, **105** (2022) 054138.
- [51] VAN KAMPEN N. and OPPENHEIM I., *Physica A: Statistical Mechanics and its Applications*, **138** (1986) 231.
- [52] SPECK T. and SEIFERT U., *Phys. Rev. E*, **70** (2004) 066112.